Direct Observation of a Hydrogen Atom Adduct to O-4 in Uracil. Energetics and Kinetics of Uracil Radicals

Jill K. Wolken and František Tureček*

Department of Chemistry, Bagley Hall, Box 351700, University of Washington, Seattle, Washington 98195-1700

Received: April 10, 2001; In Final Form: July 6, 2001

The 4-hydroxy-3,4-dihydropyrimidine-2(*1H*)-on-4-yl radical (**1**), an elusive hydrogen atom adduct to the O-4 position in uracil, was generated in the gas phase by femtosecond collisional electron transfer to O-4 protonated uracil and investigated by neutralization−reionization mass spectrometry (NRMS). A fraction of radicals **1** was stable on the 5.1 μs time scale. The main unimolecular dissociations of **1** were ring cleavages and a specific loss of the hydrogen atom from O-4, as determined by deuterium labeling. Ab initio calculations up to effective QCISD(T)/6-311+G(3df,2p) and combined density functional theory and perturbational calculations up to B3-MP2/6-311+G(3df,2p) were used to obtain bond dissociation and transition state energies for several radical and ion dissociations. The energies were used for calculations of rate constants by RRKM and transition state theory. The dissociations observed by NRMS could not be explained by competitive reactions occurring on the potential energy surface of the ground doublet state of **1** and must to a large part originate from excited electronic states of **1** that are formed by vertical electron capture. The adiabatic ionization energy of **1** was calculated as 5.55 eV. Activation energies for hydrogen atom additions to uracil were found to inversely correlate with the addition exothermicities. The most reactive position in uracil was C-5 which was calculated to account for >95% hydrogen atom additions, followed by C-6 (<5% additions), while additions to O-2 and O-4 were kinetically negligible.

Introduction

Nucleobase residues are the prime target for attack by energetic particles in the process of radiative and oxidative DNA damage.[1] Although the kinetics of radical and electron additions to nucleobases have been studied in detail in solution and frozen matrices,[2,3] relatively little is known about the nature and intrinsic reactivity of transient nucleobase radicals that are the presumed reaction intermediates. There are currently two accepted mechanisms of nucleobase radical formation.[1,4] The first comprises direct addition to the nucleobase of small radicals (H, OH, etc.) that are formed by radiolysis of water or other chemical reactions. This mechanism has been studied extensively by experiment[3] and also by medium-level ab initio calculations that yielded relative radical energies for DNA nucleobases and uracil.[5] The rates of radical additions depend on the activation barriers that determine which of the isomeric radical intermediates are formed. The other mechanism consists of electron capture followed by protonation of the transient anion radical, resulting in net hydrogen atom addition to the nucleobase.[4] Formation of isomeric radicals then depends on the topical basicities of the oxygen, nitrogen, and carbon centers in the anion-radical intermediate.

We have shown previously for model heterocyclic molecules[6] that the process of radical formation can be reversed in the gas phase, where selective protonation is used first to produce a stable cation, which is then accelerated and neutralized by collisional electron transfer from a polarizable molecular donor (Scheme 1). Because of the short duration of the electron-transfer event (e.g., $<10^{-14}$ s for uracil ions of 119 000 m s^{-1} velocity), the radical is formed with the structure and geometry of the precursor ion.[7] Following femtosecond collisional electron transfer, unimolecular dissociations of transient nucleobase radicals are investigated on the time scale of several microseconds, and the surviving radicals and dissociation products are analyzed by mass spectrometry.[8] This neutralization−reionization mass spectrometric (NRMS) method has been used to generate a variety of transient and highly reactive species.[9]

SCHEME 1

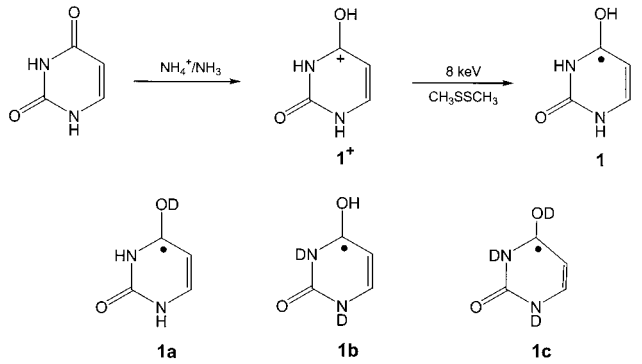

Here, we report specific preparation in the gas phase of 4-hydroxy-3,4-dihydropyrimidine-2(*1H*)-on-4-yl (**1**) derived from the RNA nucleobase uracil. Although RNA is more resistant than DNA to oxidative and other radical-induced degradation,[10] this increased stability is thought to be due to the chemical properties of the ribose moiety, rather than the presence of uracil.[11] Radical **1** can be viewed as a product of protonation at O-4 in a uracil anion-radical and thus represents a reactive intermediate of the electron capture-protonation mechanism. Previously,[12,13] we reported on the specific generation and

* To whom correspondence should be addressed. Tel.: (206) 685−2041. Fax: (206) 685−3478. E-mail: turecek@chem.washington.edu.

10.1021/jp011348z CCC: $20.00
Published on Web 08/16/2001

energetics of H atom adducts to C-5 and C-6 in uracil. In the present work, we investigate the mechanisms of radical unimolecular dissociations with the help of deuterium-labeled derivatives **1a**−**c**. The energetics of **1** and 2-hydroxy-1,2-dihydropyrimidine-4(*3H*)-on-2-yl (**2**), which is an H atom adduct to O-2 in uracil, several of their dissociation intermediates, and the corresponding cations are investigated by high-level ab initio and density functional theories. The calculated activation energies are used to assess the kinetics of unimolecular dissociations of transient uracil radicals and hydrogen atom additions in the uracil system.

Experimental Part

Materials. Uracil was purchased from Aldrich and used as received. Deuterium-labeled reagents ND_3 (Matheson, 99%D), D_2O, CD_3OD, and acetone-d_6 (all Cambridge Isotope Laboratories) were also used as received.

Methods. Measurements were carried out on a tandem quadrupole acceleration−deceleration mass spectrometer described previously.[14] Protonation by ion−molecule reactions was carried out in a tight chemical ionization (CI) source. Typical ionization conditions were as follows: electron energy 100 eV, emission current 1−2 mA, temperature 280−300 °C, ion source potential 80 V. NH_3, ND_3, acetone, CD_3COCD_3, and 2-methylpropane, water, and D_2O were used as CI reagent gases at pressures $1.0-1.5 \times 10^{-4}$ Torr as read on an ionization gauge located at the diffusion pump intake. Stable precursor ions were passed through a quadrupole mass filter operated in the radio frequency-only mode, accelerated to the total kinetic energy of 8250 eV and neutralized in the collision cell floated at −8170 V. The precursor ion lifetimes were 30−40 μs. Dimethyl disulfide (DMDS) was admitted to the differentially pumped collision cell at a pressure such as to achieve 70% transmittance of the precursor ion beam. The ions and neutrals were allowed to drift to a four segment conduit,[15] where the ions were reflected by the first segment floated at +250 V. The neutral flight times in standard NRMS measurements were 5.1 μs. The fast neutral species were reionized in the second collision cell by collision with oxygen at a pressure adjusted such as to achieve 70% transmittance of the precursor ion beam. The ions formed in the second collision cell were decelerated, energy filtered, and analyzed by a quadrupole mass filter operated at unit mass resolution. The instrument was tuned daily to maximize the ion current of reionized $CS_2^{+\bullet}$. Typically, 40 repetitive scans were accumulated per spectrum, and each spectrum was reproduced at least three times over a period of several weeks.

Collisionally activated dissociation (CAD) spectra were measured on a JEOL HX-110 double-focusing mass spectrometer of forward geometry (the electrostatic sector E precedes the magnet B). Collisions with air were monitored in the first field-free region at pressure to achieve 70% transmittance of the ion beam at 10 keV. The spectra were obtained by scanning E and B simultaneously, while maintaining a constant *B*/E ratio (B/E linked scan).

Calculations. Standard ab initio and density functional theory calculations were performed using the Gaussian 98 suite of programs.[16] Geometries were optimized using Becke's hybrid functional (B3LYP)[17] and the 6-31+G(d,p) basis set. For some species, geometries were optimized with Hartree−Fock calculations, HF/6-31G(d,p) and HF/6-31+G(d,p), as specified below. Spin-unrestricted calculations (UB3LYP and UHF) were used for open-shell systems. Spin contamination in the UB3LYP calculations was small as judged from the $\langle S^2 \rangle$ operator expectation values that were 0.75−0.77. The optimized structures were characterized by harmonic frequency analysis as local minima (all frequencies real) or first-order saddle points (one imaginary frequency). Complete optimized structures in the Cartesian coordinate format and total energies are available from the correspondence author upon request. The B3LYP/6-31+G(d,p) frequencies were scaled by 0.963 (ref 18, for other scaling factors see ref 19), the UHF/6-31G(d,p) frequencies were scaled by 0.893, and used to calculate zero-point vibrational energies (ZPVE), enthalpy corrections, and partition functions. The rigid-rotor harmonic oscillator approximation was used in all thermochemical calculations. Single-point energies were calculated at several levels of theory. In three sets of calculations, MP2(frozen core)[20] and B3LYP energies were calculated with basis sets of increasing size, e.g., 6-311+G(2d,p), 6-311+G(2df,p), and 6-311+G(3df,2p). Spin contamination in the UMP2 calculations was moderate for uracil radicals and transition states, as evidenced by the spin expectation values $\langle S^2 \rangle$ that ranged between 0.76 and 0.91. Spin annihilation using Schlegel's projection method[21] (PMP2)[16] reduced the $\langle S^2 \rangle$ values to 0.75−0.76. In addition, restricted open-shell (ROMP2) calculations[22] were carried out for the entire set of structures to deal with spin contamination.[23] The PMP2 and ROMP2 energies were averaged with the B3LYP energies according to the empirical procedure that was introduced previously[6a,b,24] and tested for several systems since.[25,26] This resulted in error cancellation and provided relative energies denoted as B3−PMP2 or B3−ROMP2,[26] as discussed below. Calculations on closed-shell systems are marked by B3-MP2. In addition a composite procedure was adopted that consisted of a single-point quadratic configuration interaction calculation,[27] QCISD(T)/6-31G(d,p), and basis set expansion up to 6-311+G(3df,2p) through PMP2 or ROMP2 single-point calculations according to eq 1:

$$\text{QCISD(T)/6-311+G(3df,2p)} \approx \text{QCISD(T)/6-31G(d,p)} + \text{MP2/6-311+G(3df,2p)} - \text{MP2/6-31G(d,p)} \quad (1)$$

This level of theory is intermediate between those of the Gaussian 2 (MP2) method[28] which uses the 6-311G(d,p) basis set in the large QCISD(T) calculation and the G2(MP2, SVP) method[29] which uses the 6-31G(d) basis set instead. We also utilized the previous finding that restricted open-shell calculations (ROMP2) provided good stabilization energies for small organic radicals.[23] Basis set expansions to effective QCISD/6-311+G(2d,p), QCISD(T)/6-311+G(2d,p), and QCISD(T)/6-311+G(2df,p) were also tested for selected systems.

Franck−Condon energies in vertical neutralization and reionization were taken as absolute differences between the total B3-MP2/6-311+G(2d,p) energies of fully optimized ion or neutral structures and those in which an electron has been added to an optimized cation structure or subtracted from an optimized neutral structure. No zero-point corrections were applied to the calculated Franck−Condon energies.

Gradient optimizations of excited-state geometries were performed with spin-unrestricted configuration interaction singles (UCIS)[30] using the 6-31+G(d,p) basis set. Improved energies for excited states were obtained from UCIS and time-dependent density functional theory[31] single-point calculations using the B3LYP hybrid functional and the larger 6-311+G(2d,p) basis set.

RRKM calculations used Hase's program[32] that was recompiled for MS-DOS and run under Windows NT.[33] Vibrational state densities were obtained by direct count of quantum states in 2 kJ mol^{-1} steps for internal energies up to 80−120 kJ mol^{-1} above the threshold. The rotational states were treated adiabati-

TABLE 1: Collisionally Activated Dissociation Spectra of Ions 1^+ and $1a^+-1c^+$

	relative intensity[a]						relative intensity[a]				
m/z	1^+	$1a^+$	$1b^+$	$1c^{+b}$	$1c^{+c}$	*m/z*	1^+	$1a^+$	$1b^+$	$1c^{+b}$	$1c^{+c}$
115				7.5	10.6	55	0.2	0.5	0.3		
114			9.1	3.0	5.9	54	0.5	0.5	0.5	0.5	0.8
113		15.3	1.6			53	1.6	1.5	1.3	1.9	3.9
112	12.9	2.2	0.2			52	1.4	1.4	0.5	0.5	0.7
98				0.5	0.7	51	0.6	0.9	0.5	0.4	0.6
97		0.9	0.5	0.8	0.3	50		2.0			
96	7.0	8.4	4.3	12.4	10.5	46		1.4	1.6	6.0	7.7
95	2.7	2.0	0.8			45		3.1	2.9	1.4	3.6
88				0.2		44	7.2	3.1	2.1	4.4	6.0
87				1.9	1.3	43	3.5	2.9	(7.7)[d]	2.8	4.2
86		0.5	0.9	1.7	1.2	42	5.4	3.1	3.4	2.5	3.0
85		2.0	0.8	0.1		41	4.0	2.3	2.8	2.8	3.1
84	2.0	0.5				40	5.4	3.2	2.0	1.7	2.5
73				3.2	4.8	39	1.3	1.3	1.7	0.6	1.1
72		0.5	3.6	10.7	11.6	38	1.1	1.0	0.9	0.7	1.0
71	0.2	8.6	4.2	1.3	3.5	32				0.5	
70	14.5	5.3	4.4	7.8	7.1	31		0.6	2.1	0.2	
69	6.1	5.5	3.5	4.2	5.6	30	0.4	0.9	0.6	1.0	1.0
68	6.5	3.9	1.6	1.5	3.3	29	1.3	1.4	2.7	3.0	3.7
67	1.7	1.2	0.6	0.5	1.0	28	5.4	2.9	1.1	0.7	0.8
66	0.4	0.5	0.2			27	0.8	0.6	1.2	0.2	
60			1.6	0.7		26	0.7	0.7	0.7	0.5	
59		0.5	(12.7)[d]	0.2		25	0.3		0.3	0.2	
58		0.5	2.3	4.9	6.8	16				0.3	
57	3.3	5.0	0.8			15	0.4		(1.1)[d]	0.2	
56	0.8	0.5	0.3			14			0.5		

[a] Relative to the sum of CAD ion intensities. [b] From protonation-exchange with D_3O^+/D_2O. [c] From protonation-exchange with ND_4^+/ND_3. [d] These peaks contained contributions from dissociations of an acetone condensation product, $C_6H_{11}O_2^+$, at *m/z* 115.

cally[34] and the microscopic rate constants, $k(E,J,K)$, were Boltzmann-averaged over the thermal distribution of rotational J and K states pertaining to the ion source temperature. Thermal rate constants were calculated using the standard transition state theory formulas.[35] The activation energies were taken from single-point calculations and the partition functions were calculated from the B3LYP/6-31+G(d,p) moments of inertia and scaled harmonic frequencies using the rigid rotor-harmonic oscillator approximation.

Results and Discussion

Ion Structures and Energetics. Because gas-phase cations served as precursors of radical **1** and its deuterium-labeled derivatives **1a**−**1c**, the chemistry and energetics of the corresponding cations $\mathbf{1}^+$ and $\mathbf{1a}^+-\mathbf{1c}^+$ are presented and discussed first. Cation $\mathbf{1}^+$ was generated by gas-phase protonation of uracil (**3**). According to the calculated topical proton affinities (PA) in uracil,[36] gas-phase acids BH^+ with PA(B) > 820 kJ mol^{-1} should protonate uracil selectively at the most basic site (O-4) to give $\mathbf{1}^+$ as the sole product. The topical proton affinity of O-4 in uracil is 857 kJ mol^{-1},[36,37] suggesting NH_4^+ (PA(NH_3) = 853 kJ mol^{-1}) and $(CH_3)_2C{=}OH^+$ (PA(acetone) = 821 kJ mol^{-1}) to be suitable mild gas-phase acids for selective protonation at O-4. The low protonation exothermicities and multiple collisions with the reagent gas in the ion source strongly indicated that $\mathbf{1}^+$ was formed with mean internal energies close to thermal (43 kJ mol^{-1} at 523 K). To generate specifically labeled ions $\mathbf{1a}^+-\mathbf{1c}^+$ we used combinations of solution H/D exchange and gas-phase protonation and deuteronation (Scheme 2).

Ions $\mathbf{1}^+-\mathbf{1c}^+$ were characterized by CAD spectra (Table 1) that were substantially different from those of C-5 protonated uracil.[12,13] In particular $\mathbf{1}^+$ showed abundant losses of H (*m/z* 112) and NH_3 (*m/z* 96). The calculated dissociation energies of

SCHEME 2

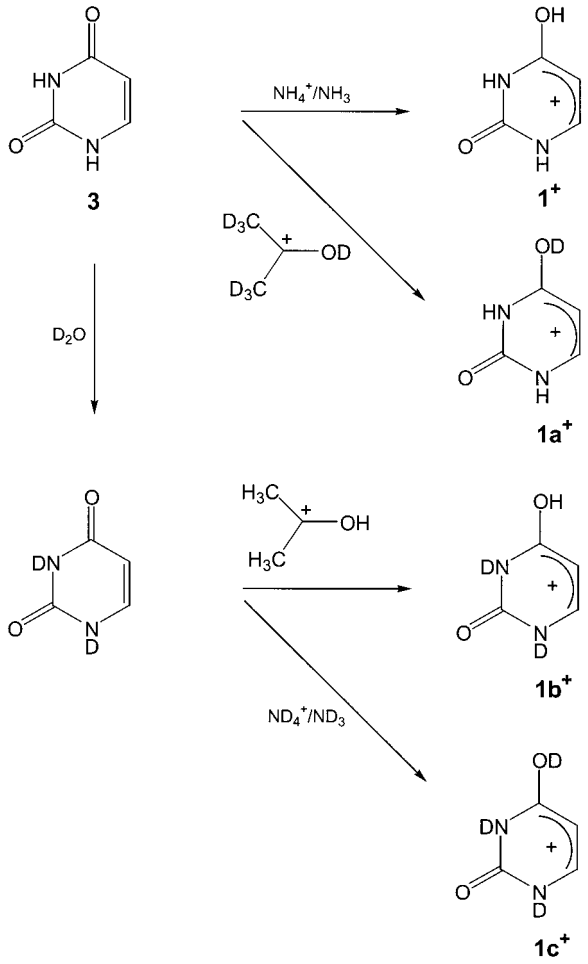

$\mathbf{1}^+$ were all substantially endothermic. The lowest-energy dissociation was a ring cleavage followed by elimination of HN=C=O to form (*Z*)-HN=CH−CH=C−OH^+ ((*Z*)-$\mathbf{4}^+$) that required $\Delta H_{r,0}$ = 347 kJ mol^{-1} (Table 2). Interestingly, the formation of *(E)*-HN=CH−CH=C−OH^+ ((*E*)-$\mathbf{4}^+$) was endothermic by 432 kJ mol^{-1}, indicating an unusually large energy difference of 85 kJ mol^{-1} for the ion *geometric* isomers. Loss of the hydrogen atom from the O-4 hydroxyl group in $\mathbf{1}^+$ to produce the uracil cation-radical ($\mathbf{3}^{+\bullet}$) required $\Delta H_{r,0}$ = 432 kJ mol^{-1}, yet it competed efficiently with the ring-cleavage dissociations (Table 1). Deuterium labeling revealed that the loss of a hydrogen atom from $\mathbf{1}^+$ involved a significant portion of hydrogens from C-5 and C-6 (Table 1), possibly via intramolecular hydrogen migrations preceding dissociation. Such hydrogen migrations are typical for high-energy dissociations in heterocyclic cations.[6c−e]

The relative energies of $\mathbf{1}^+$ and several other ion isomers have been calculated at a high level of theory recently.[36,37] In the context of the present work, we note that $\mathbf{1}^+$ is the second most stable isomer in the family of protonated uracil cations which is only 9 kJ mol^{-1} less stable than N-1 protonated 2,4-dihydroxypyrimidine, which is the most stable ion isomer.[36,37] Regarding the other relevant ion isomers, cation $\mathbf{2}^+$ is the fourth most stable ion isomer which is 31 kJ mol^{-1} less stable than $\mathbf{1}^+$.[36] It can be readily shown that an isomerization of $\mathbf{1}^+$ to $\mathbf{2}^+$ and vice versa by intramolecular proton migration must involve two four-membered transition states and therefore is likely to face a substantial energy barrier.[36] Ions $\mathbf{1}^+$ and $\mathbf{2}^+$ are therefore kinetically well stabilized against isomerization.

TABLE 2: Ion Dissociation Energies

species/reaction	basis set	energy[a] B3LYP	MP2[b]	B3-MP2[b]	QCISD[c]	QCISD(T)[c]
$\mathbf{1}^+ \rightarrow \mathbf{3}^{+\bullet} + H^\bullet$	6-31+G(d,p)	431				
	6-311+G(2d,p)	427	421 (429)[d]	424 (428)	420 (420)	421 (421)
	6-311+G(2df,p)	428	428 (435)	428 (432)	427 (426)	428 (427)
	6-311+G(3df,2p)	430	432 (439)	431 (434)	431 (431)	432 (431)
$\mathbf{1}^+ \rightarrow (Z)\text{-}\mathbf{4}^+ + HN{=}C{=}O$	6-31+G(d,p)	355				
	6-311+G(2d,p)	342	356	349	348	348
	6-311+G(2df,p)	342	356	349	348	347
	6-311+G(3df,2p)	339	354	347	346	345
$\mathbf{1}^+ \rightarrow (E)\text{-}\mathbf{4}^+ + HN{=}C{=}O$	6-31+G(d,p)	429				
	6-311+G(2d,p)	409	442	426		
	6-311+G(2df,p)	410	452	431		
	6-311+G(3df,2p)	409	454	432		

[a] In units of kJ mol^{-1} at 0 K. [b] From spin-projected MP2 energies wherever it applies. [c] From effective energies with basis sets expanded according to eq 1. [d] Energies in parentheses are from restricted open-shell MP2 calculations.

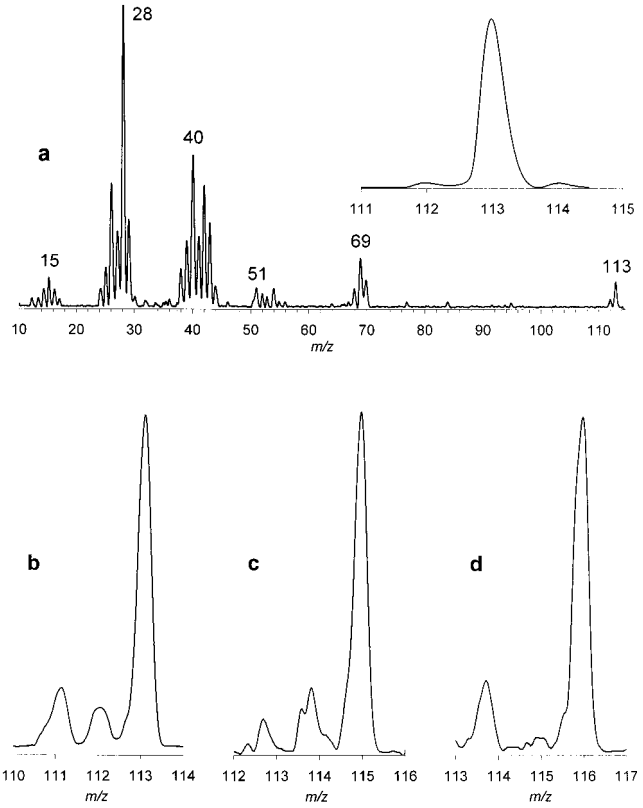

Figure 1. Neutralization (CH_3SSCH_3, 70% transmittance)-reionization (O_2, 70% transmittance) mass spectra of (a) $\mathbf{1}^+$, (b) $\mathbf{1a}^+$, (c) $\mathbf{1b}^+$, (d) $\mathbf{1c}^+$. The spectra (b)−(d) show the molecular regions only. The inset in Figure 1a shows the $(M + H)^+$ region in the CI spectrum.

Formation and Dissociations of Radical 1. Collisional neutralization of $\mathbf{1}^+$ yielded a fraction of nondissociating radicals that were detected as survivor ions at *m*/*z* 113 (Figure 1a).[8] The NR spectrum of **1** was dominated by the products of ring-cleavage dissociations, HNCO (*m*/*z* 43), $CH_2{-}CH{=}NH$ (*m*/*z* 42), CH_2CN (*m*/*z* 40), and CO and/or HNCH (*m*/*z* 28), whereas elimination of H was a relatively minor process. NR of labeled ions $\mathbf{1a}^+{-}\mathbf{1c}^+$ (Figure 1b-d) showed >85% retention of the hydrogens at C-5 and C-6 and preferential elimination of the hydrogen atom from the O-4 hydroxyl group. The latter dissociation should produce the most stable neutral uracil isomer **3**. Because loss of a hydrogen atom also occurred in $\mathbf{1}^+$ (Table 1), the neutral and post-reionization dissociations were likely to overlap on NR. The extent of ion dissociations was deconvoluted on the basis of deuterium labeling. The ion dissociations showed substantial scrambling of ring hydrogens that resulted in preferential loss of light hydrogen from $\mathbf{1a}^+{-}\mathbf{1c}^+$ (Table 1). This can be accounted for by mass balance eqs 2 and 3, where $[M - D]_{ion}$ and $[M - H]_{ion}$, respectively, are the fractions of D and H loss in pure ion dissociations, as represented by the CAD relative intensities for the particular isotopomer, α is the unknown contribution of ion dissociations in the NR mass spectrum, $[M - D]_{total}$ and $[M - H]_{total}$ are the respective observed fractions of D and H loss on NR, and $[M - D]_{radical}$ and $[M - D]_{radical}$ are the unknown fractions of D and H loss in purely radical dissociations. Fitting eq 2 with the experimental fractions for D loss from $\mathbf{1a}^+$-$\mathbf{1c}^+$ upon CAD and NR, one obtains the best fit for 21% participation of ion dissociations, and 72, 28, and >99% specificity for loss of D from O-4-D in **1a**, N-1-D and N-3-D combined in **1b**, and O-4-D, N-1-D, and N-3-D combined in **1c**, respectively.

$$[M - D]_{total} = \alpha[M - D]_{ion} + (1 - \alpha)[M - D]_{radical} \quad (2)$$

$$[M - H]_{total} = \alpha[M - H]_{ion} + (1 - \alpha)[M - H]_{radical} \quad (3)$$

This analysis further underscored the preferential loss of hydrogen atom from O-4 in neutral **1**, whereas loss from the N−H groups occurred to a lesser extent, and the C-5 and C-6 methines did not participate at all. To estimate the contribution of dissociations by H atom loss in NR, we subtracted the NR spectrum of uracil from that of **1** to eliminate the peak of reionized uracil at *m*/*z* 112. This correction accounted for 8% of the product ion intensity, indicating that the majority of peaks in the NR spectrum of **1** were due to fragments formed by ring cleavage dissociations in neutral **1** or in $\mathbf{1}^+$ following collisional ionization. The ion dissociations can be roughly gauged from the contribution of the relative intensities of the *m*/*z* 70 and *m*/*z* 44 peaks that show similar ratios in the NR and CAD spectra (Table 1). Subtraction of the CAD contributions (ca. 13% of NR peak intensities) left ca. 80% of NR fragments to be formed by ring-cleavage dissociations in neutral radical **1**.

Structure, Dissociation Energetics, and Kinetics of 1. To rationalize the unimolecular dissociations of **1** that were induced by collisional electron transfer, we performed extensive calculations of bond dissociation and related transition state energies. The optimized structure of **1** showed a nearly planar ring and standard bond lengths and angles (Figure 2). Radical **1** was the third most stable hydrogen adduct to uracil, which was 38 and 25 kJ mol^{-1}, respectively, less stable than the adducts to C-5 and C-6.[12,13] The unpaired electron in **1** was delocalized within the C-4 through C-6 allylic system, as illustrated by the calculated spin densities that were 0.41, −0.23, and 0.68 for C-4, C-5, and C-6, respectively. The unpaired electron at C-4

TABLE 3: Dissociation and Activation Energies for Uracil Radicals 1 and 2

		energy[a,b]							
		reaction[c]							
method		(1)	(2)	(3)	(4)	(5)	(6)	(7)	(8)
B3LYP/6-31+G(d,p)		92	113	180	188	26	60	97	122
B3LYP/6-311+G(2d,p)		89	112	176	186	19	56	92	116
		93[d]	107	172	185	21	53	93	112
B3LYP/6-311+G(2df,p)		89	113	178	187	18	55	93	117
B3LYP/6-311+G(3df,2p)		91	114	178	188	20.	57	94	118
PMP2/6-311+G(2d,p)		57	109	160	173	−13	54	85	103
		63[d]	116	170	184	−9	56	91	108
ROMP2/6-311+G(2d,p)		55	110	163	175	−18	57	86	104
		60[d]	119			−14	61	90	112
PMP2/6-311+G(2df,p)		58	111	162	174	−16	51	82	100
ROMP2/6-311+G(2df,p)		57	112	165	177	−21	54	83	101
PMP2/6-311+G(3df,2p)		64	114	165	177	−9	56	88	105
ROMP2/6-311+G(3df,2p)		63	116	167	180	−14	59	89	106
QCISD/6-311+G(2d,p)	PMP2	76	127	184	196	10	78	108	128
		80[d]	130	188	201	12	78	108	131
	ROMP2	79	132	187	199	10	79	109	129
		83[d]	134	192	204	12	80	108	131
QCISD/6-311+G(2df,p)	PMP2	77	128	185	197	7	75	106	125
	ROMP2	81	134	190	201	7	76	106	126
QCISD/6-311+G(3df,2p)	PMP2	83	132	188	200	14	80	111	130
	ROMP2	87	138	192	205	14	81	112	131
QCISD(T)/6-311+G(2d,p)	PMP2	68	115	170	182	5	70	98	118
	ROMP2	71	121	173	185	5	71	99	118
QCISD(T)/6-311+G(2df,p)	PMP2	69	117	171	183	2	67	95	115
	ROMP2	73	123	176	187	2	68	96	116
QCISD(T)/6-311+G(3df,2p)	PMP2	75	121	174	186	9	73	101	120
	ROMP2	79	127	178	191	9	73	102	121
B3−PMP2/6-311+G(2d,p)		73	111	168	179	3	55	89	110
		78[d]	111	170	184	6	55	92	110
B3−PMP2/6-311+G(2df,p)		74	112	170	181	1	53	87	108
B3−PMP2/6-311+G(3df,2p)		78	114	171	183	5	56	91	111

[a] In units of kJ mol^{-1} at 0 K. [b] From single-point energies on B3LYP/6-31+G(d,p) optimized geometries including zero-point vibrational energy corrections. [c] reaction 1: **1** → **3** + H•. Reaction 2: **1** → **TS1**. Reaction 3: **1** → **TS2**. Reaction 4: **1** → **TS3**. Reaction 5: **2** → **3** + H•. Reaction 6: **2** → **TS7**. Reaction 7: **2** → **TS8**. Reaction 8: **2** → **TS9**. [d] From single-point energies on HF/6-31G(d,p) optimized geometries (HF/6-31+G(d,p) for transition states) and zero-point energy corrections.

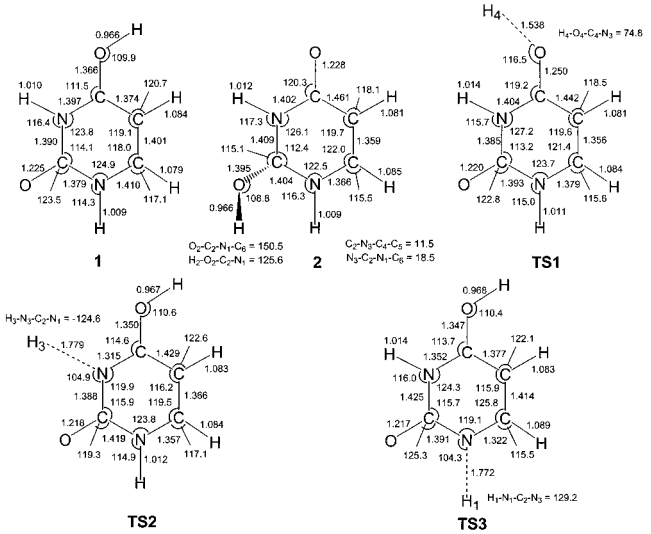

Figure 2. B3LYP/6-31+G(d,p) optimized structures of uracil radicals. Bond lengths in angstroms, bond and dihedral angles in degrees.

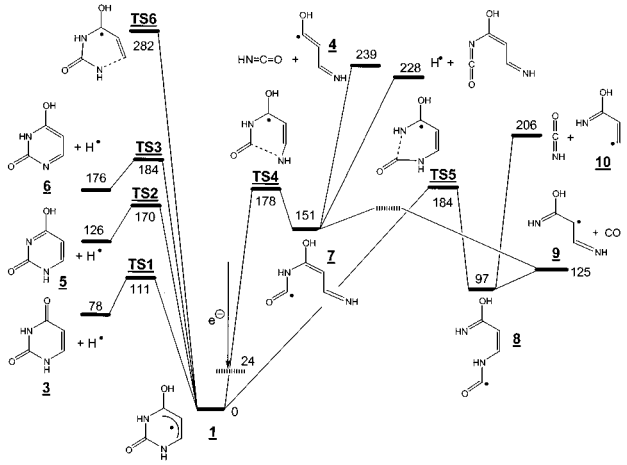

Figure 3. Potential energy diagram for dissociations of **1** from B3−PMP2/6-311+G(2d,p) calculations.

and C-6 can promote cleavage of bonds at adjacent atoms, e.g., N-1−H, N-1−C-2, O-8−H, and C-2−N-3. The energetics of these and other bond cleavages in **1** are visualized in the potential energy diagram for the ground doublet state of the radical which shows 0 K energies obtained by B3−PMP2 calculations (Figure 3), the energies obtained at other levels of theory are summarized in Table 3. Cleavage of the O-4−H bond was the lowest energy dissociation of **1** to form the most stable uracil tautomer **3**. By comparison, cleavages of the N-1−H and N-3−H bonds were 60−74 kJ mol^{-1} more endothermic to form the less stable uracil tautomers **5** and **6**, respectively. Note that the O-4−H, N-3−H, and N-1−H bonds dissociations proceeded through transition states (**TS1**, **TS2**, and **TS3**, respectively, Figure 3) that were above the corresponding product thermochemical thresholds. Note that the departing hydrogen atoms (H-4, H-1, and H-3) were situated out of the ring plane in the transition states **TS1**, **TS2**, and **TS3**, respectively (Figure 2). The existence of transition states for H eliminations from **1**

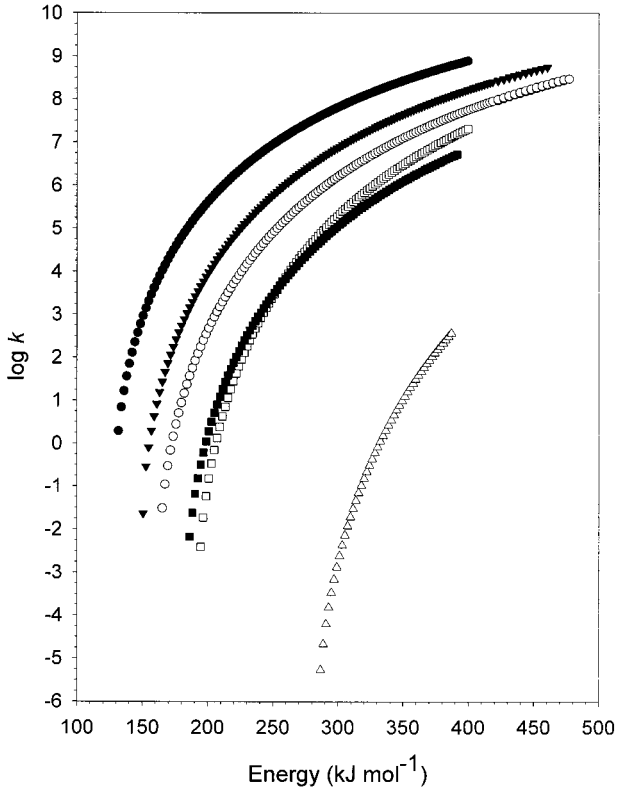

Figure 4. RRKM unimolecular rate constants for dissociations and isomerizations of **1**. Full circles: Dissociation of the O-4—H bond. Upside-down full triangles: Dissociation of the N-1—H bond. Empty circles: Dissociation of the N-3—H bond. Full squares: Ring-opening by cleavage of N-1—C-2 bond. Empty squares: Ring-opening by cleavage of the C-2—N-3 bond. Empty triangles: Ring-opening by cleavage of the N-1—C-6 bond.

indicated that that the reverse hydrogen atom additions to uracil and its tautomers **5** and **6** must also involve activation energies that affect the reaction kinetics.

Cleavages of the N-1—C-2 and C-2—N-3 bonds resulted in open-ring intermediates **7** and **8**, that were 151 and 97 kJ mol^{-1} less stable than **1**, respectively. Both ring cleavages proceeded through transition states (**TS4** and **TS5**, respectively), and required activation energies that were 67−73 kJ mol^{-1} higher than that for the H loss from O-4 (**TS1**) and comparable to that for the H loss from N-1 and N-3 (**TS2** and **TS3**, respectively, Table 3). Subsequent dissociations of **7** and **8** favored elimination of CO which converged on forming HN═C(OH)−CH═CH−NH• (**9**). The CO loss from **7** must have involved an activation barrier, because the energy threshold for the products was 26 kJ mol^{-1} below the energy of **7** which, however, was a local energy minimum. Elimination of CO from **8** was 28 kJ mol^{-1} endothermic and may involve an additional activation barrier. Eliminations of HNCO from both **7** (to form **4**) and **8** (to form **10**) were substantially endothermic, such that the respective product threshold energies were 239 and 206 kJ mol^{-1} above **1**. Cleavages of other bonds in **1** showed large transition state energies and were considered kinetically irrelevant. For example, dissociation of the vinylic N-1—C-6 bond proceeded through **TS6** that was 282 kJ mol^{-1} above **1** (Figure 3).

The differences in the transition state energies for the dissociations of radical **1** are reflected by the corresponding unimolecular rate constants obtained by RRKM calculations (Figure 4). For the 110−400 kJ mol^{-1} internal energy interval, loss of the hydrogen atom from O-4 was predicted to be 1000−10 times faster than the competing dissociations. In line with

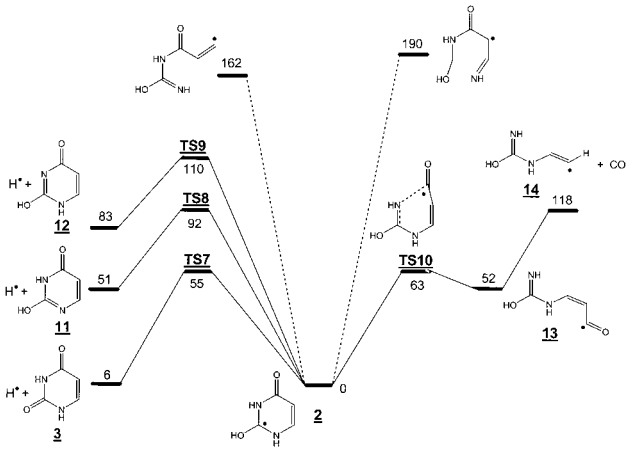

Figure 5. Potential energy diagram for dissociations of **2** from B3−PMP2/6-311+G(2d,p) calculations.

the relative magnitudes of the activation energies, loss of N-1 hydrogen atom was the second fastest reaction over the entire energy interval. Cleavages of the N-1—C-2 and C-2—N-3 bonds were competitive relative to each other, but >2 orders of magnitude slower than the fastest dissociation even in radicals possessing high internal energies.

Dissociation Energetics and Kinetics of Radical 2. Although radical **2** was not studied experimentally, its dissociation energetics was of interest for comparison with that of **1**. The dissociation and transition state energies calculated with B3−PMP2/6-311+G(2d,p) are visualized in a potential energy diagram (Figure 5), the energies obtained at other levels of theory are summarized in Table 3. Loss of the hydrogen atom from O-2 to form **3** was the energetically most favorable dissociation of **2**, which was nearly thermoneutral at the product thermochemical threshold. Eliminations of the hydrogen atoms from both N-1 and N-3 were more endothermic to produce the less stable uracil tautomers **11** and **12**. The hydrogen elimination reactions must overcome potential energy barriers; the lowest of those for the loss of H from O-2 (**TS7**) was only 55 kJ mol^{-1} above **2**. Dissociations of the N-1—H and N-3—H bonds also required transition states (**TS8** and **TS9**, respectively) that were 41 and 27 kJ mol^{-1} above the product thermochemical thresholds. Hence, hydrogen atom additions to uracil tautomers **11** and **12** were expected to require activation energies. The radical center at C-2 in **2** activates the N-3—C-4 bond whose dissociation required only 52 kJ mol^{-1} and had a transition state (**TS10**) that was 63 kJ mol^{-1} above **2**. The open-ring intermediate **13** was bound by 66 kJ mol^{-1} against elimination of CO forming the isoureidoethenyl radical **14**, which was the energetically most favorable ring cleavage dissociation of **2** that required 118 kJ mol^{-1} at the product thermochemical threshold. Cleavages of the N-1—C-6 and N-1—C-2 bonds were both substantially endothermic (Figure 5) and should not compete with the hydrogen losses on the ground-state potential energy surface.

Discussion of Radical Dissociations: The Role of Excited Electronic States. The calculated potential energy surfaces suggested that eliminations of the hydroxyl hydrogen atoms should dominate the unimolecular dissociations of uracil radicals **1** and **2**. In this discussion, we now compare the predicted dissociations with those observed for radicals generated by collisional electron transfer.

The NR dissociations of **1** showed specific loss of a hydrogen from O-4 that was not accompanied or preceded by substantial hydrogen atom migration in the ring. This observation was in keeping with the calculated transition state energies (**TS1**-**TS3**,

TABLE 4: Excited State Energies of Radicals 1 and 2

radical optimized geometry	state[d]	ΔE[a]		f[b]		$\tau(\mu s)$		configuration[c]	
		CIS[e]	TD-B3LYP[f]	CIS	TD-B3LYP	CIS	TD-B3LYP	CIS	TD-B3LYP
(*X*) 1[g]	A	4.16	2.39	0.0006	0.0006	2.2	6.7	30α → 31α	30α → 31α
	B	4.22	2.40	0.023	0.005	0.06	0.8	mixed α[h]	30α → 32α
	C	4.59	2.84	0.002	0.002	0.5	1.4	30α → 32α	30α → 33α
	D	5.17	3.40	0.000	0.000	>20	>20	30α → 33α	30α → 34α
	E	5.56	3.73	0.009	0.0015	0.08	1.1	30α → 35α	30α → 35α
(*A*) 1[i]	A	2.91	1.41	0.018	0.0046	0.2	2.5	mixed α[h]	30α → 31α
	B	3.67	2.03	0.008	0.0008	0.2	7	mixed α[h]	30α → 32α
	C	3.93	2.30	0.002	0.002	0.9	2.2	30α → 32α	30α → 33α
	D	4.40	2.83	0.0001	0.0004	12	7.2	30α → 33α	30α → 34α
	E	4.73	3.21	0.005	0.0016	0.2	1.4	mixed α[h]	30α → 35α
1+[j]	A	3.46	1.79	0.0003	0.0002	6.4	36	30α → 31α	30α → 31α
	B	3.62	1.82	0.021	0.004	0.08	1.7	mixed α[h]	30α → 32α
	C	3.94	2.27	0.0021	0.001	0.7	4.5	30α → 32α	30α → 33α
	D	4.47	2.79	0.000	0.0001	>20	30	30α → 33α	30α → 34α
	E	4.88	3.14	0.007	0.002	0.14	0.5	30α → 35α	30α → 35α

[a] Excitation energies in units of electronvolt. [b] Oscillator strengths. [c] Dominant configurations with expansion coefficients >0.85. [d] All doublet states. [e] From spin unrestricted UCIS/6-311+G(2d,p) single-point calculations. [f] From time-dependent UB3LYP/6-311+G(2d,p) single-point calculations. [g] UB3LYP/6-31+G(d,p) optimized geometry of the ground electronic state. [h] Configurations consisting of several α electron excitations. [i] UCIS/6-31+G(d,p) optimized geometry of the excited *A* state. [j] B3LYP/6-31+G(d,p) optimized geometry of the cation.

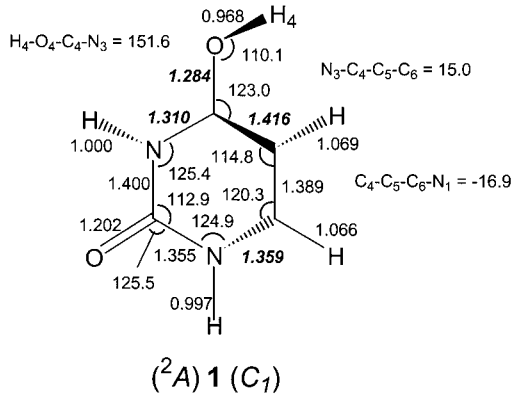

Figure 6. CIS/6-31+G(d,p) optimized geometry of the ^2A electronic state of **1** CIS/6-31+G(d,p) optimized geometries Bold italic numerals indicate bond lengths that underwent significant changes upon $^2X \rightarrow {}^2A$ electron excitation.

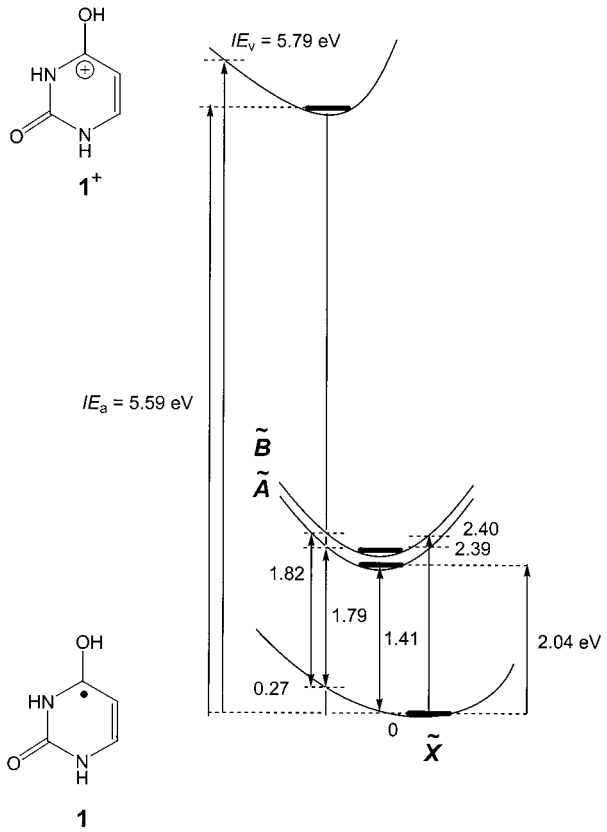

Figure 7. TD-B3LYP/6-311+G(2d,p) excitation and B3−PMP2/6-311+G(2d,p) ionization energies of **1**.

Figure 3) and relative rate constants for the loss of H from the different positions in **1** (Figure 4). However, the calculated rate constants further indicated that ring cleavage dissociations should not compete efficiently with the loss of H-4, which was in sharp contrast with NR dissociations of **1** in which ring-cleavage dissociations producing HN=C=O and CH_2CH=NH accounted for about 80% products. Another question related to the NR dissociations concerned the internal energy in the radicals formed by collisional electron transfer that drove the observed dissociations. We have shown previously for related heterocyclic radicals[6a,6b] that the vibrational energy in the species that was formed in the *ground electronic state* was convoluted from the internal energy of the precursor cation and the Franck−Condon energy acquired upon vertical electron transfer. The internal energy in ground-state **1** can be estimated as follows. The precursor ion $\mathbf{1}^+$ had an estimated 43 kJ mol^{-1} mean internal energy when formed by mildly exothermic protonation and nearly thermalized at 523 K in the high-pressure ion source. The Franck−Condon effects in vertical neutralization of $\mathbf{1}^+$ were calculated to be small, e.g., $E_{FC} = 24$ kJ mol^{-1}. Hence, the mean energy in **1** can be estimated to be close to $43 + 24 = 67$ kJ mol^{-1}. This is much less than the 111−121 kJ mol^{-1} needed to overcome the transition state for the lowest-energy dissociation by loss of hydrogen atom from O-4 (**TS1**), and entirely insufficient to access the transition state for the lowest energy ring-cleavage (**TS4**, 178 kJ mol^{-1}). The 80% of ring-cleavage dissociations in NR of **1** were therefore incompatible with the vibrational energy of the ground electronic state.

Vertical electron capture in ion $\mathbf{1}^+$ can result in the formation of excited electronic states, that can drive highly endothermic dissociations, as reported for several systems recently.[6a,6b,12,38] In the following section we investigate computationally the excitation energies in **1**.

Excited States of 1. The energies, radiative lifetimes, and dominant configurations of the five lowest excited states in **1** are given in Table 4. According to TD-B3LYP calculations,

TABLE 5: Rate Constants for H Atom Additions to Uracil

		B3−ROMP2		QCISD	QCISD(T)	
position		6-311+G(2d,p)	6-311+G(3df,2p)	6-311+G(2d,p)	6-311+G(2d,p)	6-311+G(3df,2p)
C-5	log $k_{add,200}$	8.40[b]	8.70	7.12	7.33	7.84 (7.80)[a]
	log $k_{add,298}$	9.89	10.09	9.03	9.18	9.52 (9.49)
	% at 200 K[c]	98.5	98.8	98.8	98.9	99.2 (99.0)
	% at 298 K[c]	94.3	95.1	95.2	95.5	96.2 (95.7)
C-6	log $k_{add,200}$	6.58	6.78	5.19	5.36	5.75 (5.80)
	log $k_{add,298}$	8.67	8.80	7.74	7.85	8.11 (8.14)
	% at 200 K	1.5	1.2	1.2	1.1	0.8 (1.0)
	% at 298 K	5.6	4.9	4.8	4.5	3.8 (4.3)
O-4	log $k_{add,200}$	2.59	2.88	−0.42	0.47	1.02 (0.34)
	log $k_{add,298}$	6.03	6.23	4.01	4.61	4.98 (4.52)
	% at 200 K	0.00	0.00	0.00	0.00	0.00 (0.00)
	% at 298 K	0.01	0.01	0.00	0.00	0.00 (0.00)
O-2	log $k_{add,200}$	−1.75	−1.50	−5.04	−4.26	−3.76 (−3.94)
	log $k_{add,298}$	3.08	3.25	0.88	1.40	1.74 (1.61)
	% at 200 K	0.00	0.00	0.00	0.00	0.00 (0.00)
	% at 298 K	0.00	0.00	0.00	0.00	0.00 (0.00)

[a] From effective QCISD(T) calculations using ROMP2 energies. [b] Rate constants in $cm^3\ mol^{-1}\ s^{-1}$. [c] Fractions of additions at the indicated temperatures.

TABLE 6: Energy Correlations for Hydrogen Atom Additions and Dissociations in Uracil Radicals

	energy[a]									
	C-5		C-6		O-8		O-7			
method	E_{add}[b]	E_{diss}[c]	E_{add}	E_{diss}	E_{add}	E_{diss}	E_{add}	E_{diss}	r_{lin}^2	r_{quadr}^2
B3−PMP2/6-311+G(2d,p)	16.8	113.6	22.5	103.4	38.0	72.8	52.0	3.0	0.944[d]	1.000[e]
B3−ROMP2/6-311+G(2d,p)	16.9	111.4	23.9	100.8	39.4	71.8	55.9	0.7	0.944	1.000
B3−PMP2/6-311+G(2df,p)	17.0	110.2	22.8	99.9	37.9	73.7	52.2	0.7	0.921	0.999
B3−ROMP2/6-311+G(2df,p)	17.0	108.2	24.4	97.5	39.3	72.9	56.1	−1.6	0.927	0.999
B3−PMP2/6-311+G(3df,2p)	15.7	112.9	21.8	102.0	36.8	77.7	51.0	5.5	0.914	0.998
B3−ROMP2/6-311+G(3df,2p)	15.8	110.9	23.1	99.6	38.3	77.0	54.9	3.2	0.919	0.999
QCISD/6-311+G(2d,p)/PMP2	21.8	122.3	29.2	111.8	50.9	75.9	68.4	9.7	0.949	1.000
QCISD/6-311+G(2d,p)/ROMP2	22.1	122.5	29.2	112.0	53.4	79.0	69.0	9.9	0.909	0.998
QCISD(T)/6-311+G(2d,p)/PMP2	21.0	113.5	28.6	101.9	47.5	68.0	65.4	5.0	0.965	1.000
QCISD(T)/6-311+G(2d,p)/ROMP2	21.2	113.7	28.5	102.1	50.0	71.1	66.1	4.9	0.928	0.998
QCISD/6-311+G(2df,p)/PMP2	22.1	117.5	29.6	106.8	50.7	77.3	68.6	6.8	0.926	0.999
QCISD/6-311+G(2df,p)/ROMP2	22.2	118.0	29.3	107.4	53.2	80.3	69.3	6.7	0.877	0.995
QCISD(T)/6-311+G(2df,p)/PMP2	21.3	108.7	29.0	96.9	47.3	69.3	65.6	1.9	0.945	0.999
QCISD(T)/6-311+G(2df,p)/ROMP2	21.4	109.2	28.7	97.5	49.8	72.9	66.3	1.9	0.895	0.994
QCISD/6-311+G(3df,2p)/PMP2	19.9	122.5	27.7	111.0	48.8	83.1	66.5	14.0	0.922	0.998
QCISD/6-311+G(3df,2p)/ROMP2	20.0	122.9	27.5	111.6	51.4	86.9	67.2	14.0	0.864	0.993
QCISD(T)/6-311+G(3df,2p)/PMP2	19.0	113.7	27.1	101.1	45.4	75.2	63.5	9.2	0.941	0.998
QCISD(T)/6-311+G(3df,2p)/ROMP2	19.2	114.1	26.9	101.7	48.0	78.9	64.2	9.1	0.887	0.992

[a] At 0 K in units of kJ mol^{-1}. [b] Activation energies for H atom addition to the specified position in uracil. [c] Bond dissociation energy defined as H_0(uracil) + H_0(H) − H_0(reactant). [d] Correlation coeffient for linear least-squares fit. [e] Correlation coeffient for quadratic least-squares fit.

the ^2A through ^2E excited states of **1** all had energies close to or above those for the H-loss and ring-cleavage dissociations in ground state **1**. Hence, internal conversion from an excited electronic state to the ground state can provide vibrational energy to drive these dissociations. The radiative lifetimes in vertically formed ^2A through ^2E states were in the μs range, indicating that the excited states were long-lived. Vibrational excitation caused by Franck−Condon effects was small in the ^2A state formed by vertical electron capture (Figure 7), so that most of the vibrational modes in (^2A)**1** can be expected to be in the same states as in the cation precursor.[39] Similar conclusions can be drawn for the ^2B and higher excited electronic states of **1**.[40] Hence, radiative transitions from the relaxed geometries of the excited states of **1** were also of interest. For (^2A)**1**, the corresponding radiative lifetime in the relaxed geometry was in the μs range (Table 4), allowing for internal conversion to the ground state or state-specific dissociations. The potential for the latter was indicated by the optimized geometry of the ^2A state, which showed an elongated C-4−C-5 bond and shortened C-4−O-4 and N-3−C-4 bonds (Figure 6) compared to the same parameters of the ground-state structure (Figure 2). Hence, ring cleavage by dissociation of the C-4−C-5 bond may be facilitated in the ^2A state.

Kinetics of Hydrogen Atom Addition to Uracil. The calculated activation energies for H atom additions[12,13] were further used to obtain bimolecular rate constants (k_{add}) under thermal conditions at the high pressure limit. Not surprisingly, the absolute rate constants depended critically on the activation energies, so that the values for k_{add} calculated at different levels of theory differed by 1−2 orders of magnitude (Table 5). However, the *relative rate constants* for competitive additions of H to the different positions in uracil showed a consistent pattern regardless of the level of theory used to obtain the activation energies (Table 5). At all levels of theory, C-5 was the most reactive position toward H atom addition. At 200 K, addition to C-5 is predicted to be 99% specific to yield the 5,6-dihydropyrimidine-2,4(*1H,3H*)-dion-6-yl radical **15** as the sole product.[13] At 298 K, addition to C-5 remained the dominant channel (95%) that was accompanied by addition to C-6 (5%) to form 5,6-dihydropyrimidine-2,4(*1H,3H*)-dion-5-yl radical **16**. Additions to O-4 to form **1** and O-2 to form **2** were too slow to compete with the formation of **15** and **16**. Interestingly, the activation energies for the hydrogen atom additions showed an inverse correlation with the corresponding C−H or O−H bond dissociation energies.[25,41] The correlation was best expressed by quadratic fits that gave, for example, a 0.005 kJ mol^{-1} root-

mean-square deviation (rmsd) for the B3−PMP2/6-311+G(2d,p) activation energies for H atom additions to O-2, O-4, C-5, and C-6 (Table 6). Linear fits were less tight and showed deviations $\geq$4.0 kJ mol^{-1} rmsd for activation and bond dissociation energies calculated at different levels of theory (Table 6).

Conclusions

The elusive hydrogen atom adduct to the O-4 position in uracil was generated in the gas phase and found to be stable. Specific loss of hydrogen from the O-4 hydroxyl in radical **1** was observed in accord with the calculated transition state energies and RRKM dissociation rate constants. In addition, abundant ring-cleavage dissociations occurred in the radicals that resulted in expulsion of HNCO and CO. The ring-cleavage dissociations were impossible to explain from the properties of the potential energy surface of the ground doublet state of **1** but could occur from excited electronic states produced by vertical electron capture. The kinetics of hydrogen atom additions to uracil under thermal conditions favors C-5 as the most likely site of attack.

Acknowledgment. Support of this work by NSF (Grants Nos. CHE-9712570 and CHE-0090930) is gratefully acknowledged. Computational facilities used in this work were supported by NSF (Grant CHE-9808182) and the University of Washington. Thanks are due to Dr. Martin Sadilek for assistance with CAD spectra measurements.

References and Notes

(1) von Sonntag, C. In *Physical and Chemical Mechanism in Molecular Radiation* Biology; Glass, W. A., Varma, M. N., Eds.; Plenum Press: New York, 1991; pp 287−321.

(2) Steenken, S. *Chem. Rev.* **1989**, *89*, 503.

(3) (a) Henriksen, T.; Snipes, W. *J. Chem. Phys.* **1970**, *52*, 1997. (b) Box, H. C.; Budzinski, E. E. *J. Chem. Phys.* **1975**, *62*, 197. (c) Sagstuen, E.; Hole, E. O.; Nelson, W. H.; Close, D. M. *J. Phys. Chem.* **1989**, *93*, 5974. (d) Ohta, N.; Tanaka, N.; Ito, S. *J. Chem. Soc. Perkin Trans. 2* **1999**, 2597.

(4) Symons, M. C. R. *J. Chem. Soc., Faraday Trans. 1* **1987**, *83*, 1.

(5) Colson, A.-O.; Becker, D.; Eliezer, I.; Sevilla, M. D. *J. Phys. Chem. A,* **1997**, *101*, 8935.

(6) (a) Wolken, J. K.; Turecek, F. *J. Am. Chem. Soc.* **1999**, *121*, 6010. (b) Wolken, J. K.; Turecek, F. *J. Phys. Chem. A,* **1999**, *103*, 6268. (c) Nguyen, V. Q.; Turecek, F. *J. Am. Chem. Soc.* **1997**, *119*, 2280. (d) Nguyen, V. Q.; Turecek, F. *J. Mass Spectrom.* **1997**, *32*, 55. (e) Nguyen, V. Q.; Turecek, F. *J. Mass Spectrom.* **1996**, *31*, 1173.

(7) Holmes, J. L. *Mass Spectrom. Rev.* **1989**, *8*, 513.

(8) Turecek, F. *J. Mass Spectrom.* **1998**, *33*, 779.

(9) For most recent reviews, see: (a) Zagorevskii, D. V.; Holmes, J. L. *Mass Spectrom.* Rev. **1999**, *18*, 87. (b) Schalley, C. A.; Hornung, G.; Schroder, D.; Schwarz, H. *Chem. Soc. Rev.* **1998**, *27*, 91.

(10) Thorp, H. H. *Chem. Biol.* **2000**, *7*, R33.

(11) Chatgilialoglu, C.; Ferreri, C.; Bazzanini, R.; Guerra, M.; Choi, S.-Y.; Emanuel, C. J.; Hoerner, J. H.; Newcomb, M. *J. Am. Chem. Soc.* **2000**, *122*, 9525.

(12) Syrstad, E. A.; Vivekananda, S.; Turecek, F. *J. Phys. Chem. A* **2001**, *105*, 8339.

(13) Wolken, J. K.; Sysrstad, E. A.; Vivekananda, S.; Turecek, F. *J. Am. Chem. Soc.* **2001**, *123*, 5804.

(14) Turecek, F.; Gu, M.; Shaffer, S. A. *J. Am. Soc. Mass Spectrom.* **1992**, *3*, 493.

(15) Turecek, F. *Org. Mass Spectrom.* **1992**, *27*, 1087.

(16) Frisch, M. J.; Trucks, G. W.; Schlegel, H. B.; Scuseria, G. E.; Robb, M. A.; Cheeseman, J. R.; Zakrzewski, V. G.; Montgomery, J. A., Jr.; Stratmann, R. E.; Burant, J. C.; Dapprich, S.; Millam, J. M.; Daniels, A. D.; Kudin, K. N.; Strain, M. C.; Farkas, O.; Tomasi, J.; Barone, V.; Cossi, M.; Cammi, R.; Mennucci, B.; Pomelli, C.; Adamo, C.; Clifford, S.; Ochterski, J.;. Petersson, G. A.; Ayala, P. Y.; Cui, Q.; Morokuma, K.; Malick, D. K.; Rabuck, A. D.; Raghavachari, K.; Foresman, J. B.; Cioslowski, J.; Ortiz, J. V.; Stefanov, B. B.; Liu, G.; Liashenko, A.; Piskorz, P.; Komaromi, I.; Gomperts, R.; Martin, R. L.; Fox, D. J.; Keith, T.; Al-Laham, M. A.; Peng, C. Y.; Nanayakkara, A.; Gonzalez, C.; Challacombe, M.; Gill, P. M. W.; Johnson, B. G.; Chen, W.; Wong, M. W.; Andres, J. L.; Head-Gordon, M.; Replogle, E. S.; Pople, J. A. *Gaussian 98, Revision A.6*, Gaussian, Inc., Pittsburgh, PA, 1998.

(17) (a) Becke, A. D. *J. Chem. Phys.* **1993**, *98*, 1372, 5648. (b) Stephens, P. J.; Devlin, F. J.; Chablowski, C. F.; Frisch, M. J. *J. Phys. Chem.* **1994**, *98*, 11 623.

(18) Rauhut, G.; Pulay, P. *J. Phys. Chem.* **1995**, *99*, 3093.

(19) (a) Finley, J. W.; Stephens, P. J. *J. Mol. Struct.* (*THEOCHEM*) **1995**, *357*, 225. (b) Wong, M. W. *Chem. Phys. Lett.* **1996**, *256*, 391. (c) Scott, A. P.; Radom, L. *J. Phys. Chem.* **1996**, *100*, 16 502.

(20) Møller, C.; Plesset, M. S. *Phys. Rev.* **1934**, *46*, 618.

(21) (a) Schlegel, H. B. *J. Chem. Phys.* **1986**, *84*, 4530. (b) Mayer, I. *Adv. Quantum Chem.* **1980**, *12*, 189.

(22) McWeeny, R.; Diercksen, G. *J. Chem. Phys.* **1968**, *49*, 4852.

(23) Parkinson, C. J.; Mayer, P. M.; Radom, L. *J. Chem. Soc., Perkin Trans. 2*, **1999**, 2305.

(24) Turecek, F. *J. Phys. Chem. A* **1998**, *102*, 4703.

(25) (a) Turecek, F.; Wolken, J. K. *J. Phys. Chem. A* **1999**, *103*, 1905. (b) Turecek, F.; Carpenter, F. H. *J. Chem. Soc., Perkin Trans. 2* **1999**, 2315. (c) Turecek, F.; Polasek, M.; Frank, A. J.; Sadilek, M. *J. Am. Chem. Soc.* **2000**, *122*, 2361.

(26) Rablen, P. R. *J. Am. Chem. Soc.* **2000**, *122*, 357.

(27) Pople, J. A.; Head-Gordon, M.; Raghavachari, K. *J. Chem. Phys.* **1987**, *87*, 5968.

(28) Curtiss, L. A.; Raghavachari, K.; Pople, J. A. *J. Chem. Phys.* **1993**, *98*, 1293.

(29) (a) Curtiss, L. A.; Redfern, P. C.; Smith, B. J.; Radom, L. *J. Chem. Phys.* **1996**, *104*, 5148. (b) Smith, B. J.; Radom, L. *J. Phys. Chem.* **1995**, *99*, 6468.

(30) Foresman, J. B.; Head-Gordon, M.; Pople, J. A.; Frisch, M. J. *J. Phys. Chem.* **1992**, *96*, 135.

(31) Stratmann, R. E.; Scuseria, G. E.; Frisch, M. J. *J. Chem. Phys.* **1998**, *109*, 8218.

(32) Zhu, L.; Hase, W. L. *Quantum Chemistry Program Exchange*; Indiana University: Bloomington, IN, 1994. Program No. QCPE 644.

(33) Frank, A. J.; Sadilek, M.; Ferrier, J. G.; Turecek, F. *J. Am. Chem. Soc.* **1997**, *119*, 12343.

(34) Zhu, L.; Hase, W. L. *Chem. Phys. Lett.* **1990**, *175*, 117.

(35) Levine, I. N. *Physical Chemistry*, 3rd ed.; McGraw-Hill: New York, 1988; p 839.

(36) Wolken, J. K.; Turecek, F. *J. Am. Soc. Mass Spectrom.* **2000**, *11*, 1065.

(37) Podolyan, Y.; Gorb, L.; Leszczynski, J. *J. Phys. Chem. A* **2000**, *104*, 7346.

(38) (a) Polasek, M.; Turecek, F. *J. Am. Chem. Soc.* **2000**, *122*, 9511. (b) Frank, A. J.; Turecek, F. *J. Phys. Chem. A* **1999**, *103*, 5348. (c) Nguyen, V. Q.; Sadilek, M.; Frank, A. J.; Ferrier, J. G.; Turecek, F. *J. Phys. Chem. A* **1997**, *101*, 3789.

(39) Dunbar, R. C. *J. Chem. Phys.* **1989**, *90*, 7369.

(40) This follows from the fact that as the electron is promoted to higher excited states and becomes less tightly bound, the excited state geometry of the radical resembles more closely that of the ion. Hence, Franck−Condon effects on vertical electron capture diminish when higher excited states of the radical are formed.

(41) (a) Evans, M. G.; Polanyi, M. *Trans. Faraday Soc.* **1938**, *34*, 11. (b) Butler, E. T.; Polanyi, M. *Trans. Faraday Soc.* **1943**, *39*, 19.